Catalysis Today 394-396 (2022) 475–485

Contents lists available at ScienceDirect

Catalysis Today

journal homepage: www.elsevier.com/locate/cattod

Catalytic pyrolysis of used tires on noble-metal-based catalysts to obtain high-value chemicals: Reaction pathways

Paula Osorio-Vargas [a,b,*], Cristian H. Campos [c], Cecilia C. Torres [d], Carla Herrera [c], Krishnamoorthy Shanmugaraj [c], Tatiana M. Bustamante [c], J.N. Diaz de Leon [e], Francisco Medina [f], Luis E. Arteaga-Pérez [a,g,*]

[a] Laboratory of Thermal and Catalytic Processes (LPTC-UBB), Universidad del Bío-Bío, Facultad de Ingeniería, Departamento de Ingeniería en Maderas, Concepción, Chile
[b] Centro de Investigación y Desarrollo en Ciencias Aplicadas "Dr. J.J. Ronco" (CINDECA), Departamento de Química, Facultad de Ciencias Exactas, UNLP-CCT La Plata, CONICET, 47 No. 257, 1900 La Plata, Buenos Aires, Argentina
[c] Universidad de Concepción, Facultad de Ciencias Químicas, Departamento de Físico-Química, Edmundo Larenas 129, Concepción, Chile
[d] Departamento de Ciencias Químicas, Facultad de Ciencias Exactas, Universidad Andres Bello, Sede Concepción, Autopista Concepción-Talcahuano, 7100 Talcahuano, Chile
[e] Centro de Nanociencias y Nanotecnología, Universidad Autónoma de México, Ensenada, B.C., Mexico
[f] Laboratorio de Cromatografía, Centro de Biomateriales y Nanotecnología, Universidad del Bio-Bio, Concepción, Chile
[g] Universidad de Concepción, Unidad de Desarrollo Tecnológico, Coronel, Chile

ARTICLE INFO

Keywords:
Waste tires
Catalytic pyrolysis
Noble metal
Titanate nanotubes
BTX

ABSTRACT

A systematic study on the use of noble metals (Pd, Pt, Au) supported on titanate nanotubes (NT-Ti) for selectively producing BTX and p-cymene from waste tire pyrolysis is provided here. All the materials were characterized for chemical, textural and structural properties using a range of analytical techniques. The M/NT-Ti (M: Pd, Pt, or Au) catalysts exhibit low nanoparticle sizes (1.8 <NPs<2.2 nm), and a homogeneous pore size distribution. The catalysts demonstrated excellent activity for converting WT into BTX-enriched oil when tested in a micro-pyrolysis system coupled to chromatography/mass spectrometry (Py–GC/MS). The BTX production was enhanced by the presence of catalysts with a selectivity order as follows Pd > Pt ≈ Au > support > non-catalyst. The Py-GC/MS suggest that the catalysts participate in the secondary reactions of dealkylation, dehydrogenation, isomerization, aromatization, and cyclization leading to a higher formation of BTX than the uncatalyzed reaction. Finally, a comprehensive reaction pathway describing the catalytic pyrolysis of WT over Pd/NT-Ti was proposed by studying the catalytic pyrolysis of individual polymers constituting the waste tires, and D,L-Limonene.

1. Introduction

Recent estimations report that billions of used tires (WT) are wasted every year (25.7 million tons) causing environmental, and health problems [1]. The waste tires are difficult to *dispose of* due to the huge rate of generation (increasing every year) and their intrinsic properties (not susceptible to auto-degradation). Nowadays, there are well-established alternatives to dispose of waste tires, such as tire retreading, mechanical lapping, rubber recovering, incineration and others. The most traditional treatment for valorizing waste tires as an energy source is based on its combustion (around 32 MJ kg^{-1} heating value), which is recognized as a low-value polluting process. Therefore, efforts are being made to valorize the waste tires into a series of marketable products with different applications, for example: recycling into concrete and road construction materials [2], chemical platforms [3], and novel adsorbents [4]. In the endeavor for fractionating WTs into a higher value product, thermochemical decomposition via pyrolysis has emerged as a promising process. The pyrolysis consists of the thermochemical transformation (in the absence of oxygen) of the tire's polymeric fraction: natural rubber (NR), styrene-butadiene rubber (SBR), and butadiene rubber (BR) into three major fractions: A **Liquid** (35–65%, TPO) containing aliphatic and aromatic hydrocarbons,

* Corresponding authors at: Laboratory of Thermal and Catalytic Processes (LPTC-UBB), Universidad del Bío-Bío, Facultad de Ingeniería, Departamento de Ingeniería en Maderas, Concepción, Chile.
E-mail addresses: posorio@ubiobio.cl (P. Osorio-Vargas), larteaga@ubiobio.cl (L.E. Arteaga-Pérez).

https://doi.org/10.1016/j.cattod.2021.06.029
Received 15 March 2021; Received in revised form 31 May 2021; Accepted 25 June 2021
Available online 12 July 2021

Table 1
Compositional analysis of WT samples.

Elemental composition (wt%)					Elemental composition (mg kg^{-1})					Proximate analysis (wt%)				
C	H	O[a]	N	S	Al	Ca	Fe	K	Na	MC	VM	FC	Ash	[b]HHV(MJ Kg^{-1})
79.5	7.33	1.32	0.47	1.48	1352	1152	1117	509	508	1.2	58.8	30.2	9.9	36.6

[a] By difference, O = 100-C-H-N-S-A
[b] HHV (MJ/kg) = 35.2 C + 116.2 H + 6.3 N + 10.5 S - 11.1 O, where C, H, O, S, N are fractional elemental composition of carbon, hydrogen and oxygen, respectively

heteroatomic compounds, etc. A **Solid** (12–45%, rCB) with exceptional properties to be used as a selective adsorbent or reused for tires production, and a **Gas** (10–35%, TPG) which is usually used as a heat source (50 MJ kg^{-1}).

Among the high-value compounds that can be found in the TPO are DL-limonene, isoprene, benzene, toluene, mixed-xylene, ethylbenzene, styrene, p-cymene, and some polycyclic aromatic hydrocarbons [3,5,6]. However, these compounds are difficult to exploit as marketable products because they are present in a complex mixture with similar physical properties so that it is very difficult to separate them using conventional distillation methods. Accordingly, many studies have been carried out seeking to produce an upgraded TPO by controlling the product distribution during the pyrolysis. For example, if selectivity towards aromatic hydrocarbons such as benzene, toluene, mixed-xylene, and ethylbenzene (BTXE) is enhanced, a fuel grade TPO can be produced [3,5]. Indeed, the TPO-derived fuels have several advantages from petroleum-derived fuels, as it mitigates the environmental problems generated by their conventional production process (extraction/oil refining), while opens new business opportunities in the recycling and waste management sector. Morever, the valorization of WTs into BTXEs-enriched fuel is an interesting opportunity from the circular economy viewpoint.

William et al. [7] published one of the pioneering studies for producing upgraded TPO via catalytic pyrolysis of waste tires. Their objective was to maximize the concentration of monoaromatics compounds in TPO by employing zeolite catalysts with different acidity and pore size (ZSM-5 and Y-zeolite). The largest pore size and lowest Si/Al ratio were the most influential properties during upgraded TPO production, leading to the highest aromatic hydrocarbon content. Since that time, many publications using zeolites-based catalysts to enhance the selectivity to single-ring aromatic compounds are being published [8–17]. These works have a common conclusion that acidity/basicity, pore channel size and structure, and Si/Al ratio would affect aromatics production during WT pyrolysis over zeolites. However, in many cases, the monoaromatics were produced along with undesirable polyaromatic hydrocarbons (PAHs) and with a considerable coke deposition, which hindered the stability and selectivity of the zeolite-based catalyst [18–20]. Boxiong et al. [11,12] showed that both PAHs and coke were promoted by large pore size and lower Si/Al ratio in USY zeolites, causing their short-term deactivation.

One of the solutions that have arisen to the problems mentioned above was reported by Jitkarnka et al. [21], who intended to improve the activity and selectivity of zeolites by loading Ni on HZSM-5, HMOR, HY, and HBETA, respectively. They found that the presence of Ni in HMOR zeolite strongly favored the selective formation of monoaromatics and olefins while di-, poly-, and polar-aromatics were reduced. On the contrary, the Ni/HBETA catalyst incremented the formation of heavy components. However, this last result was attributed to zeolite properties, such as channel structure and density of acid sites, and no major attention was paid to the role of metallic sites.

Besides zeolites, noble metals-based catalysts have also been evaluated for WTs pyrolysis. In fact, these materials have demonstrated to be active for pyrolysis while proving a narrower product distribution and a lower content of polycyclic and polar aromatics than the zeolites. In this sense, the participation of ruthenium in the pyrolysis reaction was studied in Ru/SBA-1 and Ru/MCM-4 catalysts [18,19]. Authors reported that, in addition to increased gaseous products, the Ru sites were also active in reducing PAHs. The Ru/SBA-1 catalyst with the smallest mean particle size (2.56 nm) and a strong interaction Ru-support resulted in a higher activity toward reducing PAHs compounds and resistance to coke formation. In general, the observed activity was attributed to the high dispersion of metal, its hydrogenation capacity, and the support acidity. In fact, the role of the metal sites during WTs pyrolysis was inspected in a previous study by using Ni, Co, and Pd supported over inert support (SiO_2) for the catalyzed pyrolysis of waste tires. The Pd/SiO_2 catalyst was the most selective to aromatic compounds such as BTXs, and p-cymene, which was ascribed to the well-known hydrogenation/dehydrogenation ability of Pd sites. These results suggest that the aromatization and cyclization reactions taking place during the pyrolysis are affected by metal sites as well as by the support nature (mostly acidity). Accordingly, the use of wisely designed acid supports (i.e., nanostructured oxides) could be an attractive way for generating highly dispersed catalysts with a bifunctional character, which could aid in producing an upgraded TPO from WT pyrolysis.

Therefore, this work conducts a study of the catalytic pyrolysis of waste tires on noble-metal-based catalysts (Pd, Pt, and Au) supported on titanate nanotubes for the selective production of valuable aromatic compounds (i.e., BTXs and p-cymene). The effectivity of catalysts (measured as selectivity to aromatics) was evaluated with respect to the non-catalyzed reaction in a Py-GC/MS system. In order to get deep insights into the transformation behavior and reaction pathways, the catalytic pyrolysis was also carried out on individual rubbers (Polyisoprene, Polybutadiene, and Styrene-Butadiene) and DL-limonene, since this latter has been identified as a precursor of aromatic compounds [6,14,16,22–24]. Finally, we have proposed a plausible reaction route for aromatics (BTX and p-cymene) formation from waste tires.

2. Materials and methods

2.1. Raw materials

The used tire samples were collected as granules, crushed, and sieved into particle sizes between 180 and 300 μm. The pure elastomers: cis-1,4-polyisoprene (IR), cis-polybutadiene (BR), and styrene-butadiene (SBR), were supplied by Sigma-Aldrich (Chile) and pre-processed in a similar way as the WT. Moreover, the DL-limonene (≥95.0%, CAS Number 138-86-3), benzene (≥99.9%, CAS Number 71-43-2), toluene (≥99.9%, CAS Number 108-88-3), o-xylene (≥99.0%, CAS Number 95-47-6), m-xylene (≥99.5%, CAS Number 108-38-3), p-xylene (≥99.5%, CAS Number 106-42-3) and p-cymene (≥99.5%, CAS Number 99-87-6), K_2PtCl_4 (CAS Number 10025-99-7), and $AuCl_4$ (CAS Number 16961-25-4) were purchased from Sigma-Aldrich (Chile) and metal precursor $PdCl_2$ was purchased from Merck (Chile). TiO_2 nanoparticles (anatase, nanopowder, particle size <25 nm, BET surface area 45–55 m^2 g^{-1}).

2.2. Characterization of waste tires

The raw material (waste tire) was analyzed for elemental composition in a Leco CHNS 628 elemental analyzer according to the ASTM D3172 Standard method. The proximate analysis was achieved in a muffle furnace (Thermo Scientific F6020C) following the ASTM D3172 standard method. The composition of inorganic elements was

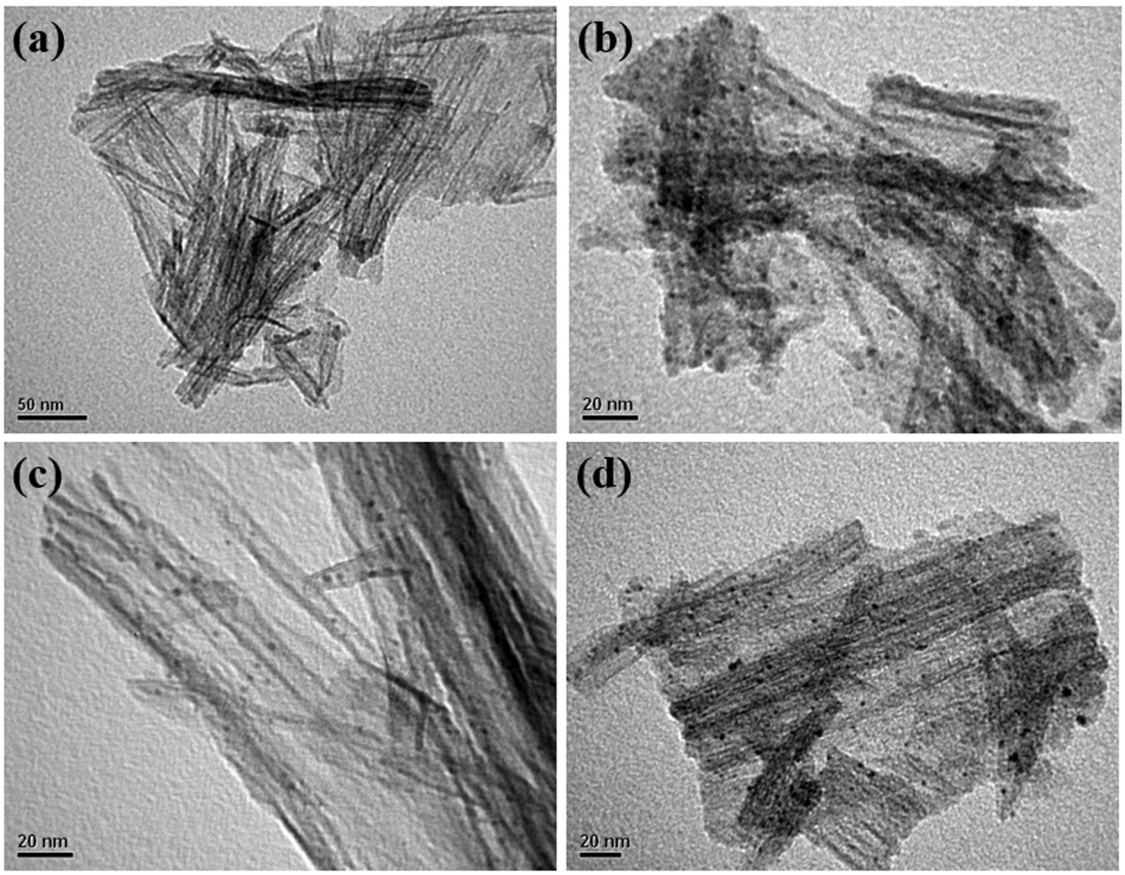

Fig. 1. TEM micrographs of (a) pristine-Ti-nanotubes, (b) Pd/NT-Ti, (c) Pt/NT-Ti and (d) Au/NT-Ti catalysts.

determined by inductively coupled plasma optical emission spectrometry (ICP-OES) using a PerkinElmer Optima 7000 DV ICP-OES series instrument. The weight loss of tires as a function of temperature (TGA) and the differential thermal analysis (DTA) were recorded using a thermobalance (Netzsch, model STA 409 PC) in a temperature range from 20 °C to 650 °C at a heating rate of 20 °C min^{-1} and using N_2 as the carrier gas. Compositional information of the WT samples is provided in Table 1.

2.3. Catalyst synthesis and characterization

2.3.1. Preparation of the supports and catalysts

The supports of titanates nanotubes (NT-Ti) were prepared according to the protocol described in a previous study [25,26]. The supported noble metals catalysts were prepared for generating 1 wt% of Pd, Pt, or Au, on the Ti-nanotubes. Briefly, the support (1.0 g) was dispersed in 150 mL of distilled water using an ultrasonic treatment for 15 min. Further, a sufficient amount of methanolic solution of metal precursor ($PdCl_2$ K_2PtCl_4 or $AuCl_4$) was added to the above-dispersed solution and stirred for 4 h. Then, 2 mL of a freshly prepared aqueous solution of 0.1 mol L^{-1} of $NaBH_4$ was added to the above mixture with continuous stirring for another 45 min. The resulting solid dispersion was centrifuged and washed several times with distilled water and absolute ethanol three times. Finally, the obtained solid was dried at 50 °C for 5 h. The catalysts were labeled as M/NT-Ti (M: Pd, Pt, or Au).

2.3.2. Characterization

The surface areas and pore structures of the catalysts were measured by nitrogen adsorption-desorption isotherms using a Micromeritics ASAP 2010 system. Chemical analysis was performed by inductively coupled plasma-mass spectrometry on an ICP-MS spectrometer Perkin Elmer Elas 6000. Transmission electron microscopy (TEM) images were obtained on a JEOL model of JEM-1200 EX II microscope. The catalysts were dispersed in ethanol in an ultrasound bath for approximately 5 min, deposited on a carbon-coated copper grid, and air-dried before imaging. The surface acidity of solid materials was measured by potentiometric titration of a catalyst suspension in acetonitrile with n-butylamine, using an Ag/AgCl electrode [27]. In a typical run, 0.1 g of the solid was stirred in acetonitrile for 3 h, and the contents were titrated with a solution of 0.1 N n-butylamine in acetonitrile at a flow rate of 0.02 mL min^{-1}. The electrode potential variation was periodically registered. The total acidity (meq n-butylamine/g catalyst) and the acidic strength (mV) were estimated from potentiometric curves (See Fig. S1). The XPS spectra of the catalysts were recorded using a SPECS® spectrometer with a PHOIBOS® 150 WAL hemispherical energy analyzer having an angular resolution less than 0.5° that are equipped with XR 50 Al-X-ray and μ-FOCUS 500 X-ray monochromator (Al excitation line $h\nu = 1486.6$ eV) sources. The binding energy (BE) peaks were referenced to the C 1s peak (284.8 eV) to account for the charging effects. Mixed Gaussian/Lorentzian functions were used to fit the spectrum after background subtraction according to the Shirley equation [28]. Surface atomic ratios were calculated from the ratios of peak area normalized by the corresponding atomic sensitivity factors that were provided by the software.

2.4. Pyrolysis coupled to mass spectrometry experiments (Py-GC/MS)

The fast catalytic pyrolysis of WTs was carried out in an analytical micro-pyrolysis reactor (CDS5200, CDS Analytical Co Ltd.) connected in line with a gas chromatograph equipped with a mass spectrometer system, GC/MS (Clarus 690, QS8. Perkin Elmer). The pyrolysis reactor consists of a quartz tube (length = 2 cm and ID = 2 mm) which is placed

Table 2
Physicochemical characterization data obtained of the synthesized materials.

Material	Metal loading (%)	S_{BET} (m^2/g)	d_{pore} (nm)	V_{pore} (cm^3/g STP)	Metal d_{TEM} (nm)	Acid strength (mV)	Total acidity (meq g^{-1})
NT-Ti	–	358	6.30	0.64	–	155.1	2.29
Pd/NT-Ti	0.92	105	3.84	0.27	1.8 ± 0.4	82.9	2.15
Pt/NT-Ti	0.89	228	4.25	0.41	2.2 ± 0.2	-22.2	2.01
Au/NT-Ti	0.95	238	4.31	0.42	1.9 ± 0.1	-126.0	0.59

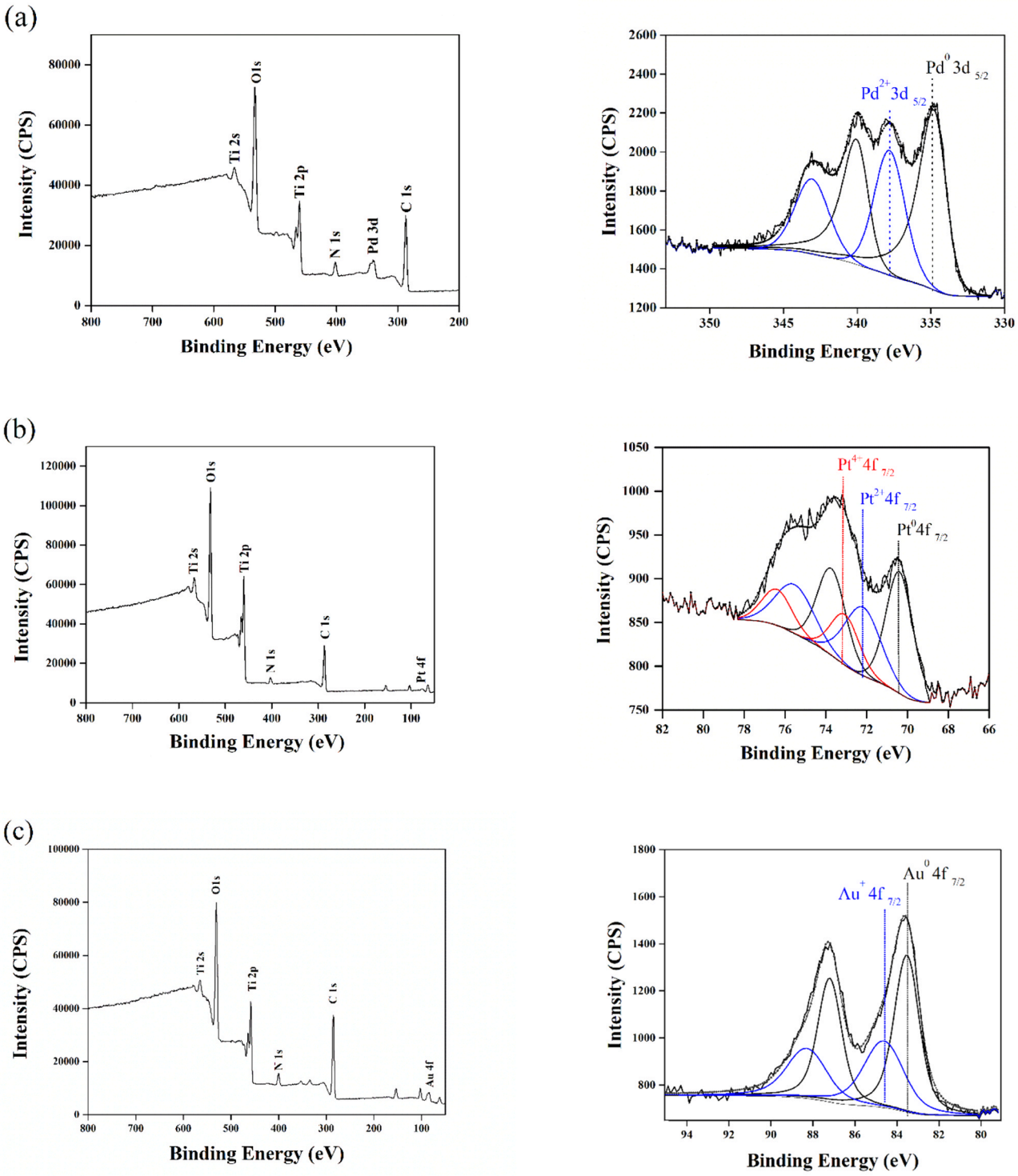

Fig. 2. X-ray photoelectron spectra (XPS) spectra of Pd 3d and Pt 4f and Au 4f for the as-synthesized (a) Pd/NT-Ti, (b) Pt/NT-Ti, and (c) Au/NT-Ti catalysts.

within a platinum filament (heating element). In a typical experiment, about 1 ± 0.1 mg (AD 6000 Ultra MicroBalance Perkin Elmer) of raw material (used tire, IR, BR and SBR) was placed in the middle of the reactor separated from the catalyst (in both sides) by quartz wool (See Fig. S2). The catalysts to feedstocks mass ratio was held at 1:4 and it was distributed on both sides of the reactor to avoid leakage. Inspired in our previous findings, the experiments were performed at two temperatures, 400 and 450 °C and using high purity He as carrier gas (pure 99.996%, BOC) [22,29]. The heating rate used was 2000 °C s^{-1}, and the dwell time was 20 s. For experiments of DL-limonene catalytic conversion, the liquid sample (1 mg) was absorbed in quartz wool and placed in the middle of the reactor. Then, the reaction conditions and product analysis were set as the same as pyrolysis. The reaction products were separated in an Elite 1701 column (30 m × 0.25 mm × 0.25 μm) heated from 45° to 280 °C at 2.5 °C min^{-1}. Then the compounds were analyzed by MS, and the identification was made by the match-degree between their mass spectra and the NIST MS library database. Because the amount of sample was strictly controlled, the relative peak area ($Area_{compound(i)}/Area_{All\ identified\ compounds}$) was used to determine the product distribution. The specific amounts of BTX, p-cymene, and limonene were quantified by calibration curves ($R^2 > 0.995$) prepared for each analytical standard (benzene, toluene, o-xylene, m-xylene, p-xylene, and p-cymene) following the method reported in [30]. For an adequate comparison of catalysts effect, the yield of each compound was calculated as:

$$Yield\ \ of\ \ compound(i) = \frac{mass\ \ of\ \ compound\ \ (i)}{(initial\ \ mass\ \ of\ \ WT * X_{WT})} x100 \qquad (1)$$

Here, X_{WT} is the fractional conversion of the WT, calculated as: $(m_{oWT} - m_{fWT})/ m_{oWT}$. The m_{oWT} and m_{fWT} are the mass of waste tires loaded into the reactor and the final solid residue after the reaction.

3. Results and discussion

3.1. Waste tires characterization

WT thermal decomposition was evaluated by TGA and DTG analysis, as is shown in Fig. S3. The maximum mass loss achieved was 62% observed between 200 and 530 °C. Deconvolution treatment indicates that decomposition can be divided into three stages related to different decomposition temperatures of components of WT. The first peak at approximately 350 °C was ascribed to degradation of NR, while second peak between 350 and 415 °C can be assigned to the decomposition of both NR and SBR in agreement with previous studies [31,32]. In this stage is observed the maximum loss mass approximately at 380 °C. Finally, the loss of mass at around 440 °C can be attributed to the decomposition of the two rubbers SBR and BR.

3.2. Catalysts characterization

The morphology and structure of the prepared catalysts were characterized by TEM. The TEM images (Fig. 1) and XRD patterns confirm that the hydrothermal synthesis of the support was successful. The typical pattern for titanates nanotubes 2θ = 24.7°, 28°, and 48° were observed (See Fig. S4) [33]. The NT-Ti have an average length of 69.0 ± 46.8 nm and an external diameter of 6.4 ± 2.9 nm, which are similar to the dimensions mentioned in our previous work [25,26]. For the supported Pt, Pd, and Au catalysts, all of them exhibit homogeneously distributed NPs within the inner surface of the Ti-nanotubes, as shown by TEM images (Fig. 1) and particle size distribution (See Fig. S5). The nanotubes shape and size were not modified after the metal deposition, while the metallic NPs were loaded mainly on the inner surfaces of the support. Furthermore, small particle sizes were obtained in the three catalysts. The sizes for Pd, Pt, and Au NPs were approximately 1.8 ± 0.4 nm, 2.2 ± 0.2 nm, and 1.9 ± 0.1 nm, respectively. These results support that the synthesis method promoted a more controlled inner surface deposition, enhancing the catalyst homogeneous noble metal nanoparticles dispersion.

Table 3
XPS characterization for the noble metal-supported catalysts.

Catalyst	Ti $2p_{3/2}$ (eV)	Pd $3d_{5/2}$ (eV)		Pt 4 $f_{7/2}$ (eV)		Au 4 $f_{7/2}$ (eV)	
		Pd^0	Pd^{2+}	Pt^0	$Pt^{2+,4+}$	Au^0	Au^+
Pd/NT-Ti	458.2	334.7 (42)	337.8 (58)	–	–	–	–
Pt/NT-Ti	458.2	–	–	70.4 (45)	72.9 (55)	–	–
Au/NT-Ti	458.1	–	–	–	–	83.7 (60)	84.8 (40)

Metal loadings were analyzed by the ICP measurements, and these results are summarized in Table 2. The nominal metal and experimental contents were similar, indicating that no substantial metal loss during the synthesis process took place and confirming the chemical composition of the catalysts.

The surface areas and pore distributions of support and catalysts obtained from the nitrogen adsorption-desorption isotherms at −196 °C were analyzed as shown in Table 2. The surface area, pore size, and pore volume of all the catalysts decreased compared to those of the pristine NT-Ti. However, independent of the decreases in the samples still retain a significantly high surface area for mesoporous materials. Moreover, the results confirm the favored encapsulation of the metallic NPs into the inner surface of the nanotubes. These findings are in good agreement with previous studies. The acid strength and the total acidity of the pristine and metal-supported TiO_2 nanotubes were evaluated, and the results are summarized in Table 2 and Fig. S1. The acid strength can be determined according to the criterion proposed by Cid and Pecchi [27]: $E_0 > 100$ mV, very strong sites; $0 < E_0 < 100$ mV, strong sites; $-100 < E0 < 0$ mV, weak sites and $E_0 < -100$ mV, very weak sites. According to this classification, it is observed that pristine NT-Ti exhibit an acid strength of 155.1 mV, which corresponds to strong sites; meanwhile, Pd/NT-Ti catalyst displays a strength of 82.9 mV corresponding to strong acid sites. Regarding Pt and Au, these showed an acid strength of −22.2 mV and −126.0 mV, respectively, which can be assigned to weak acid sites. Regarding total acidity, this decreased in the following order: NT-Ti > Pd/NT-Ti > Pt/NT-Ti > Au/NT-Ti. The lower total acidity verified for Au/TiNTcan be attributed to the effective creation of basic sites during the synthesis process. These results demonstrate the bifunctional character of catalysts used in this study.

On the other hand, the surface composition of the prepared catalysts was characterized by the XPS, as shown in Fig. 2. The chemical composition of the metallic species is resumed in Table 3. In all the catalysts, no residual Na, B, or chloride species were detected by XPS, which indicates the removal of chlorides and Na during catalyst preparation. Fig. 2(a) shows XPS survey of Pd//NT-Ti catalyst. The high-resolution XPS spectrum for Pd was deconvoluted in two groups of signals. The first signal corresponds to the presence of Pd^0 for Pd $3d_{5/2}$ and Pd $3d_{3/2}$ at 334.7 and 340.2 eV, respectively [34]. The second signal contains other peaks at 337.8 and 343.1 eV that correspond to Pd^{2+} [34]. Based on this information, we propose that the Pd precursor was not completely reduced after the reduction treatment with $NaBH_4$. According to the metallic BE, the percentage of the Pd^0 was calculated based on the integration of its individual components to the total amount of Pd, given a 42% of Pd is in a metallic state.

The Pt//NT-Ti catalysts exhibit an XPS survey and high-resolution XPS spectrum for Pt 4f with the signals for the Pt $4f_{7/2}$ and Pt 4 $f_{5/2}$ peaks corresponding to the contribution of the Pt^0, Pt^{2+}, and Pt^{4+} species, as shown in Fig. 2(b). The deconvolution generated three groups of contributions: (1) signals at 70.4 and 73.8 eV corresponding to Pt^0, (2) the peaks detected at 72.2 and 75.6 eV that are associated with Pt^{2+}, and (3) the signals at 73.2 and 76.5 that are assigned to the Pt^{4+} species [35].

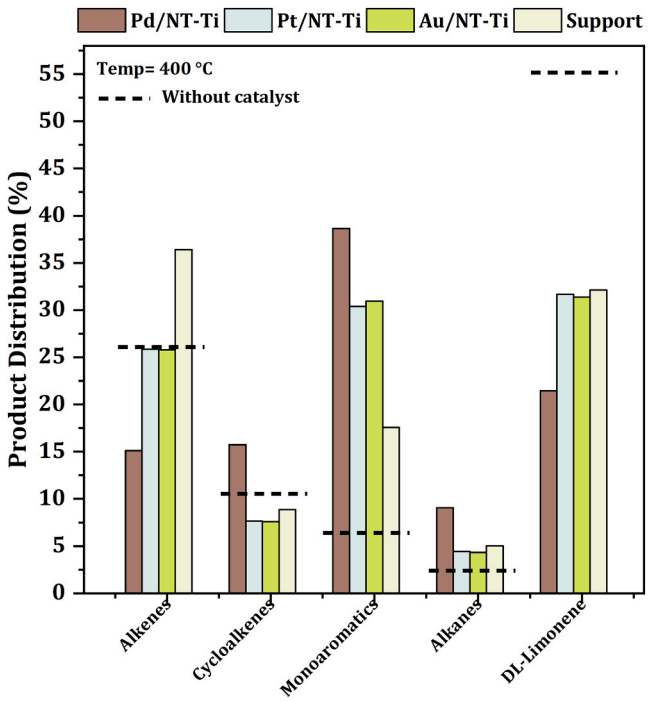

Fig. 3. Product distribution obtained from used tire pyrolysis reaction on catalysts of Pd, Pt, and Au supported on NT-Ti. Comparison with reaction without catalyst.

These measured spectral lines suggest that the Pt NPs are partially reduced to the metallic state after the reduction treatment with $NaBH_4$.

Catalyst sample Au/NT-Ti exhibited a clear Au $4f_{7/2}$ and Au $4f_{5/2}$ peak at approximately 83.7 eV and 87.3 eV (Fig. 2c), which corresponds to the pure monometallic reduced Au^0. The small peaks appearing at BE 84.8 eV and 87.3 eV are likely a result of the presence of some oxidized gold (Au^+) species arising from incomplete reduction of the catalysts during the treatment with $NaBH_4$. The percentage of the Au^0 was found that 60% in the catalysts surface. According to the XPS results, all the catalysts displayed an incomplete reduction after the reduction treatment. This behavior is in line with the work reported by Lakshmanareddy et al., in which the authors claim that during the preparation of noble metals NPs on the surface of titanate nanotubes, partial reduction of metal precursor occurs due to the possibility of the formation of multiple layers of metals ions on the surface [36].

3.3. Catalytic activity determined by Py-GC/MS analysis

3.3.1. Catalyst effect on the product distribution

The pyrolysis reaction of used tires was conducted in the presence and absence of catalyst at the temperature of highest mass loss as detected by TGA analysis (400 °C). The identified products were grouped as alkenes, alkanes, cycloalkenes, and aromatic compounds, as appear in Table S1. These were detected in both the catalyzed and non-catalyzed reactions but with different product distribution, as is shown in Fig. 3.

The main difference found in product distribution is about aromatic compounds content since, for all catalysts, this was four times higher than the value corresponding to the uncatalyzed reaction. In contrast, the selectivity to DL-limonene was much higher for the reaction without catalyst, almost twice, which could be due to the fact that secondary reactions involving limonene are favored in the catalyzed reactions. The DL-limonene can undergo isomerization, dehydrogenation, C–C bond cleavage, and aromatization reactions driving cycloalkanes, lineal alkenes, and aromatic compounds [6,14,16,22–24]. This fact could explain its lowest selectivity in the catalyzed reactions.

On the other hand, an effect of the support on secondary reactions was also observed. These reactions can be promoted over acid sites of titanates nanotubes, in which a large number of Lewis and, to a lesser extent, Bronsted acid sites have been identified [33,37]. These Bronsted acid sites were detected in the NT-Ti support and catalysts, as shown in Fig. S1 and Table 2. In addition, these sites' concentration is correlated with isolated Ti-OH groups [37], as observed here by ATR-FTIR spectra in the O-H stretching region (See Fig. S2). This fact led to a higher formation of aromatic compounds than non-catalyzed but lower than that observed with catalysts. The order of selectivity towards the formation of aromatic compounds was as follows Pd > Pt ≈ Au > support > non-catalyst.

In view of these results, the effect of catalysts on the yield and selectivity to BTX and p-cymene was evaluated (Fig. 4). A higher selectivity toward benzene was achieved on Pd/NT-Ti catalyst than for the other tested materials, while the Pt/NT-Ti and Au/NT-Ti showed a better promotion to the formation of p-cymene. Regarding the yield to these compounds, the main difference between the catalysts was also towards benzene (Fig. 4). Besides showing higher selectivity to benzene, the Pd/NT-Ti showed a higher yield of this compound than the other catalysts and the uncatalyzed reaction. Interestingly, the xylenes yield in the uncatalyzed reaction was slightly higher than in the catalyzed reactions, suggesting no effect of the catalyst in its formation. Regarding support, selectivity towards BTX and p-cymene is only marginally higher compared to the non-catalyzed reaction.

The major effect of the use of catalysts was towards the formation of p-cymene and toluene concerning non-catalyzed reaction, while the Pd/NT-Ti catalyst also promoted the formation of benzene. Reaction pathways proposed for benzene and toluene formation go through the dealkylation of p-cymene and other alkylbenzenes [22]. The former, coming from the dehydrogenation of limonene and the alkylbenzenes originated from cycloalkenes dehydrogenation. Both reactions (dealkylation and dehydrogenation) can be promoted by these metals [38,39]. Additionally, the higher yield to benzene and toluene observed in the Pd/NT-Ti catalyst with respect to other catalysts (Pt- and Au/NT-Ti) can be mainly explained due to the more significant acidity catalyst

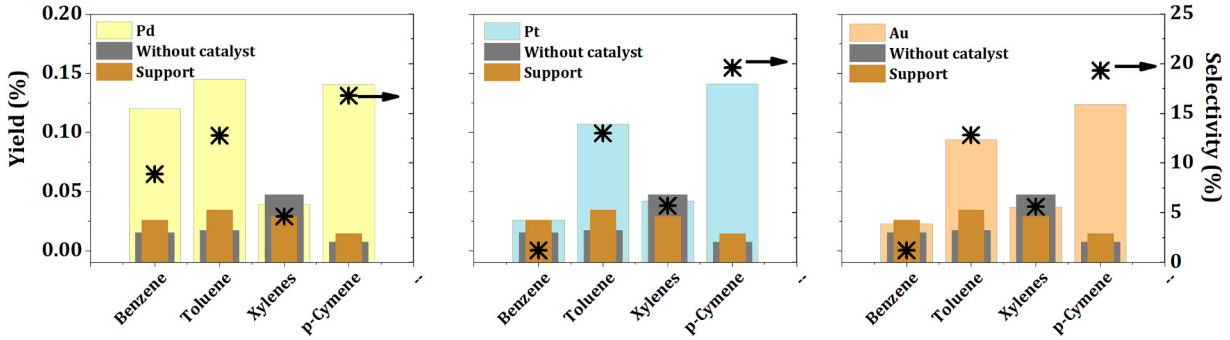

Fig. 4. Effect of using catalysts of Pd, Pt, and Au supported over NT-Ti toward the yield and selectivity of BTX and p-cymene in used tire pyrolysis.

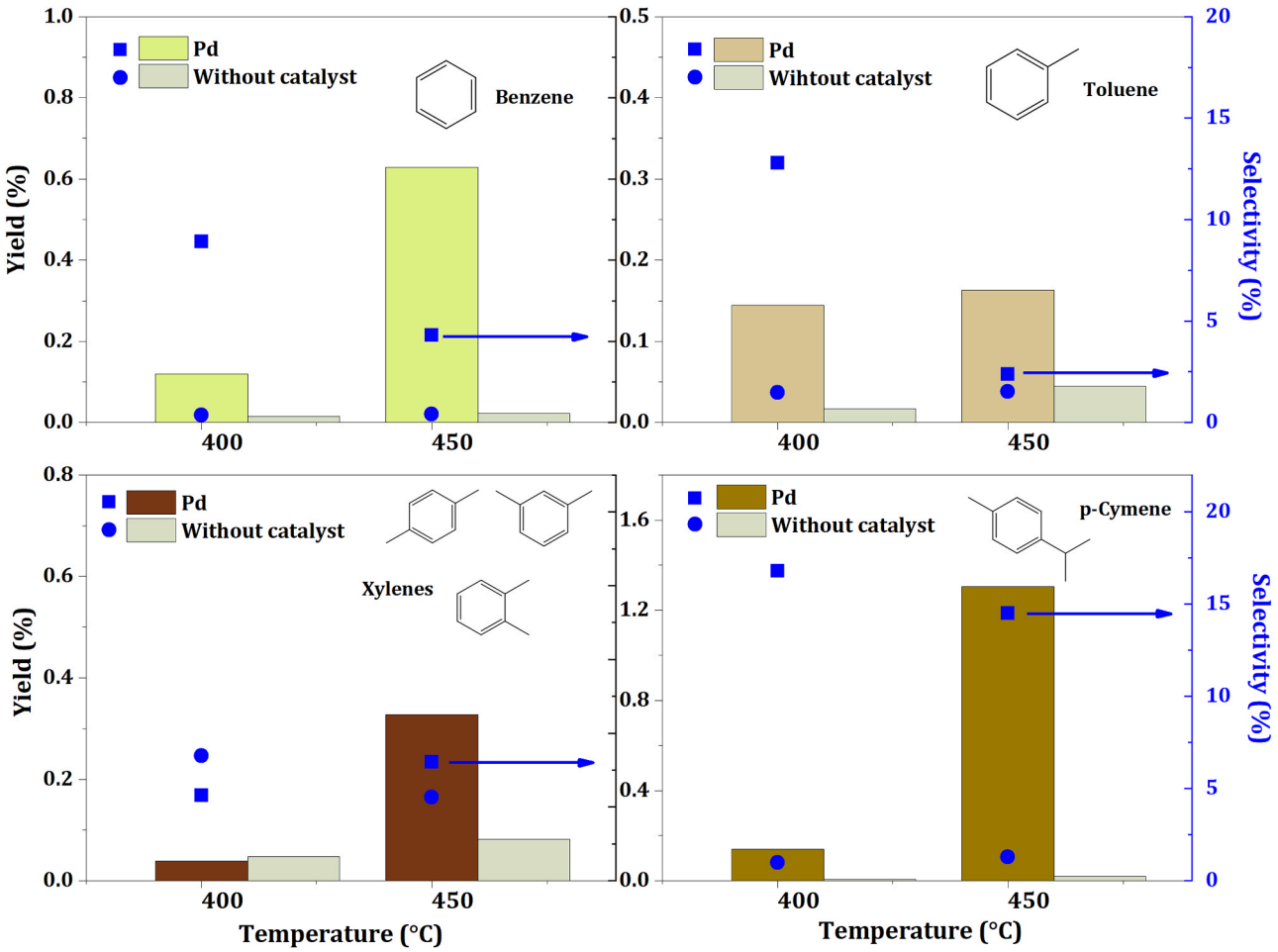

Fig. 5. Yield and selectivity to BTX and p-cymene during used tire pyrolysis in Pd/NT-Ti catalyst presence.

(Table 2). Such as has been reported [38,40], acid- and metal sites or bifunctional catalysts can promote dehydrogenation reactions. Furthermore, the BTX yield directly correlated with acid sites' content as both acidity and yield increased in the following order: Pd > Pt > Au.

3.3.2. *Effect of temperature on BTX and p-cymene formation during Pd/NT-Ti catalyzed WTP*

Fig. 5 exhibits the effect of the pyrolysis temperature on the yield and selectivity to BTX and p-cymene for catalyzed and uncatalyzed reactions. Selectivity was calculated with respect to all identified compounds. As the temperature increases, the yield of monoaromatics compounds is favored in both the catalyzed and uncatalyzed reactions. However, the production is six times fold in the catalyzed reaction. In contrast, benzene and toluene selectivity for catalyzed reaction dropped significantly, suggesting the participation of these compounds in secondary reactions with the rise of the temperature.

On the other hand, the catalyst significantly enhances p-cymene formation. According to these results, the presence of Pd/NT-Ti promoted the formation of BTX and p-cymene during waste tire pyrolysis. The yield and selectivity values suggest that Pd/NT-Ti participates in the secondary reactions of dealkylation, dehydrogenation, isomerization, aromatization, and cyclization leading to a higher formation of BTX, which could be ascribed to the well-known activity of Pd sites for these types of reactions [38–40]. Moreover, the bifunctional character of the catalyst (metal and acid sites) may have a synergistic effect on the catalytic activity since the cyclization, isomerization, and aromatization reactions may be favored both over metallic and acid sites of the catalyst [38,40]. In addition, mesoporous materials, as those used in this study,

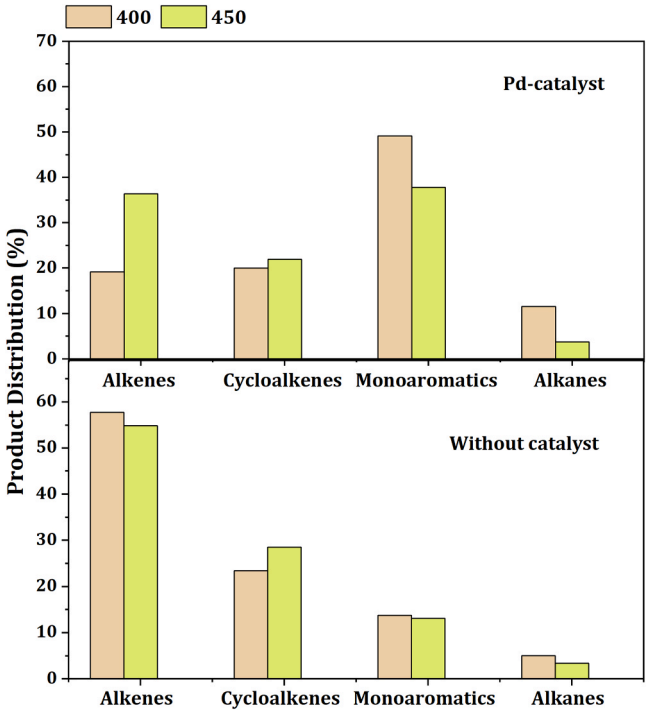

Fig. 6. Product distribution of identified products during used tire pyrolysis.

have gained increasing attention in the waste tire pyrolysis reactions since the low mass transfer rate in zeolites (catalysts more used), in some cases, favors aromatic condensation reactions forming coke deposits on active sites of catalyst [5].

The higher the temperature, the higher the BTX formation, which demonstrates that increasing the reaction temperatures favor the aromatization reactions. However, a further increase of the temperature (>600ºC) is not advisable. Under such extreme conditions, the pyrolysis reactions favor cracking reactions and some cases, the formation of PAHs and heavy polar-aromatic compounds [6,7,11,20,24,41]. In addition to decreasing the BTX content in the reaction products, the presence of PAHs can lead to catalyst deactivation [11,12,18–20]. It should be highlighted that in the present study, no PAHs were detected at any of the experimental conditions explored, which validated the hypothesis that BTX can be selectively produced over the studied catalyst.

Selectivity toward all identified compounds as a function of temperature and the presence of the catalyst is displayed in Fig. 6. At the lowest temperature, the uncatalyzed reaction is more selective towards alkenes (57.8% vs. 19.2% for Pd/NT-Ti), while in the presence of Pd/NT-Ti it is more selective towards monoaromatics (49.2% vs. 13.8 for uncatalyzed). Consequently, the behavior of the product distribution, in this case, indicates that the formation of the aromatic compounds goes through secondary reactions involving alkenes.

At the maximum reaction temperature (450 °C), a slight decrease in selectivity to monoaromatics in the catalyzed reaction and growth of alkenes was observed. These results are in agreement with those reported by [41], who indicated that increasing the temperature favors the formation of alkenes to the detriment of the production of aromatic compounds. It is worth noticing that under the experimental conditions used here, without the catalyst, the increase in temperature had no significant effect on selectivity.

The selectivity towards BTX found here over the Pd/NT-Ti catalyst was similar to those already reported using zeolites [16,17]; however, the reaction temperature was lower (400 °C), and no PAHs were detected. Previous studies have demonstrated that the formation of p-cymene during WT catalytic pyrolysis is promoted by the presence of acid sites in the catalyst [42], which could explain the role of NT-Ti during this process.

Despite the clear advantages of using Pd/NT-Ti for the selective production of BTX and p-cymene from waste tires pyrolysis, at this point is difficult to elucidate which of the reaction steps are being affected by the catalyst. Therefore, in order to shed light on such a complex reaction network, the Pd/NT-Ti catalytic pyrolysis of individual polymeric constituents in the WT was studied. Furthermore, the effect of Pd/NT-Ti on the production of aromatics from DL-limonene was evaluated by Py-GC/MS.

3.3.3. *Catalytic pyrolysis of polymeric constituents of WT (IR, BR and SBR) and DL-limonene over Pd/NT-Ti*

Aiming to elucidate possible reaction pathways ruling the WT pyrolysis, the reaction was studied at 400 ºC in a Py-GC/MS system under uncatalyzed conditions and using Pd/NT-Ti for the individual polymers constituting the tires, namely, polyisoprene rubber (IR), butadiene rubber (BR) and styrene-butadiene rubber (SBR), respectively. The products identified during these experiments are presented in Tables S2, S3, and S4 of the Supplementary material.

3.3.3.1. Pyrolysis of BR. The majoritarian product from the uncatalyzed reaction of BR was the cyclohexene, 4-ethenyl- with a selectivity of 65.2%, followed by cyclooctene, 5,6-diethenyl-, cis- and 1,3-butadiene, while no BTXs neither p-cymene were detected. When the reaction was performed in the presence of the Pd/NT-Ti, there was a significant change in the selectivity profile. In this case, the selectivity to cyclohexene, 4-ethenyl- decreased to 4.9%, and the BTEX were detected with

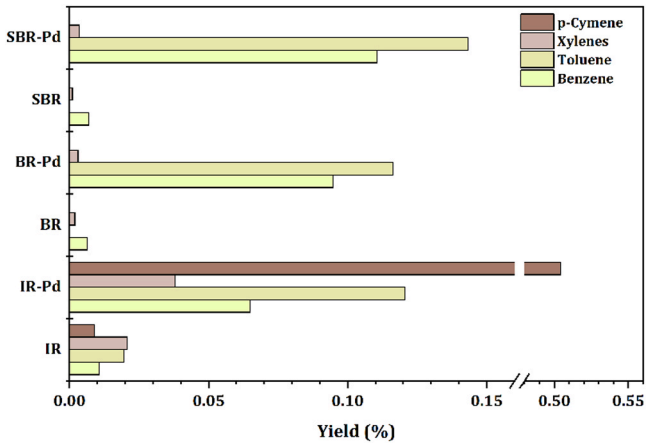

Fig. 7. Yield of BTX and p-cymene from oligomers of tire using Pd/NT-Ti.

the following selectivity order: toluene 18.5% > benzene 15.0% > ethylbenzene 8.2% > xylenes 0.7%. These results indicate that the formation of aromatic compounds from BR could be occurring from cyclohexene, 4-ethenyl- conversion. The pyrolysis of BR starts with the β-bond cleavage (primary reaction) forming an allylic radical, which rearranges as 1,3-butadiene and cyclohexene, 4-ethenyl- [43], both observed here during the non-catalyzed reaction. The cyclohexene, 4-ethenyl- is further dehydrogenated over Pd^0 sites into ethylbenzene and subsequently undergoes dealkylation reactions resulting in the observed aromatic compounds (BTX).

3.3.3.2. Pyrolysis of SBR. During the pyrolytic decomposition of SBR (without catalyst), the same majoritarian compound detected for BR was formed (cyclohexene, 4-ethyl-), in this case at 43.7% selectivity. However, it is widely accepted that the primary reactions of SBR pyrolysis lead to styrene and 1,3-butadiene [32], which were found here with a selectivity of 15.7% and 3.6%, respectively. The greater selectivity to cyclohexene, 4-ethyl- could be explained by the cyclodimerization of 1, 3-butadiene through a Diels-Alder reaction [44,45]. Similarly, as occurred with BR, the catalyzed reaction favored the formation of BTEX with a considerable decrease of the cyclohexene, 4-ethyl- of approximately 6-fold.

3.3.3.3. Pyrolysis of IR. Thermal degradation of IR has been proposed to occur through the β-bond homolytic rupture leading to the formation of two radical chains, which can undergo an intramolecular cyclization, followed by scission yielding DL-limonene and 1,5-dimethyl-5-ethenyl-cyclohexene. In addition, radicals can unzip toward the monomeric isoprene unit [22]. These reaction routes were confirmed here by the presence of these species in the products (uncatalyzed reaction) with the selectivity of 56.0% and 19.5% for DL-limonene and isoprene, respectively. When the pyrolysis was carried out in the presence of Pd/NT-Ti, the selectivity to limonene dropped almost 2-fold, and aromatic compounds appeared in the reaction products e.g., toluene, xylenes, and p-cymene. It should be noticed that p-cymene does not appeared as a product of the secondary reactions of the other elastomers. This compound can be formed from DL-limonene, one of the main products of IR degradation as mentioned before. Once DL-limonene is formed, it may be isomerized to terpinolene and α- and γ-terpinene, which were detected in the pyrolysis products. Subsequently, these terpenes can be dehydrogenated to p-cymene. All of these reactions can be promoted by acid and metallic sites or by bifunctional acid/metal catalysts [40]. Benzene and toluene detected here can come from dealkylation reactions of p-cymene and dehydrogenation of cycloalkenes.

Finally, the yield of BTX and p-cymene from the uncatalyzed and Pd/NT-Ti catalyzed pyrolysis of individual polymers is shown in Fig. 7. Such as is seen, there is a noticeable effect of the catalyst on the formation of

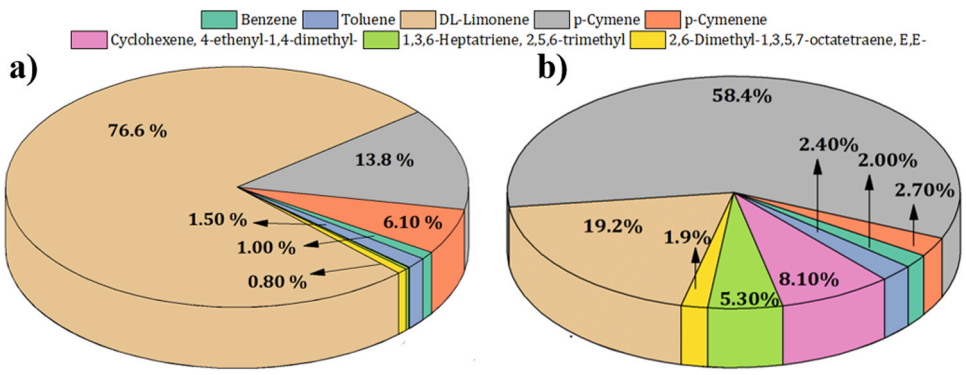

Fig. 8. Product distribution of DL-limonene pyrolysis at 400 °C under a) uncatalyzed and b) catalyzed by Pd/NT-Ti.

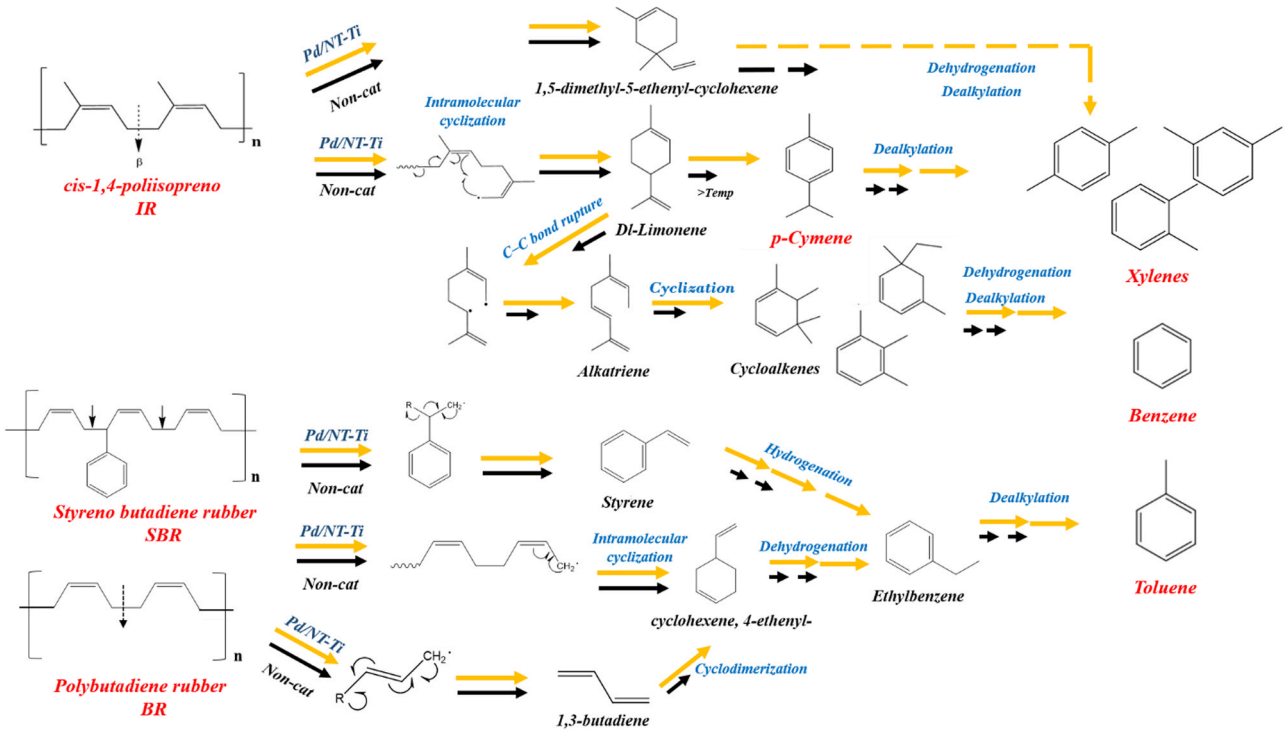

Fig. 9. Reaction pathways towards BTX and p-cymene formation from waste tire pyrolysis on Pd/NT-Ti catalyst and without catalyst. Yellow line: Catalyzed reaction, Black line: Uncatalyzed reaction.

aromatics. For example, the uncatalyzed reaction produced 5–20 times less benzene and toluene and 60 times less p-cymene than the catalyzed pyrolysis. These results along with that previously discussed, allow stating that BTX formation is promoted by the Pd/NT-Ti action in the decomposition of all the oligomers in the WT; however, the p-cymene formation can only be ascribed to the pyrolysis of polyisoprene. In fact, the results suggest that p-cymene formation can be explained by the pyrolysis of DL-limonene, which is further analyzed in the present paper.

3.3.3.4. DL-limonene pyrolysis. The results for DL-limonene uncatalyzed and Pd/NT-Ti-catalyzed pyrolysis are presented in Fig 8(a) and (b). As was confirmed, the Pd/NT-Ti promoted the formation of p-cymene, which -under catalyzed conditions- was found as the majoritarian product (58.4% selectivity). These results demonstrates that at the working temperature (400 °C), the DL-limonene pyrolysis mainly contributes to the formation of p-cymene rather than aromatics.

3.3.4. Reaction pathways towards the formation of BTX and p-cymene during Pd/NT-Ti-catalyzed pyrolysis of WT

The results from pyrolysis experiments confirmed the selective formation of cycloalkenes, alkenes, and aromatic compounds, as well as the significant effect of Pd/NT-Ti on BTX and p-cymene selectivity. These results were used as the basis for proposing reaction pathways describing WT pyrolysis over Pd/NT-Ti (Fig. 9).

Briefly, the natural rubber (cis-1,4-polyisoprene) undergoes β-bond cleavage concerning the double bonds of the main polymer chain. This radical is subsequently converted via intramolecular cyclization to form D, L-limonene, or unzipped towards the monomeric isoprene unit. Both of them were observed as the main products during the uncatalyzed pyrolysis of WT. Subsequently, reactions of isomerization and dehydrogenation occur on limonene resulting in p-cymene formation, which was considerably promoted over Pd/NT-Ti. The synthesis de p-cymene from limonene over Pd catalyst was confirmed, and the results were in agreement with that already reported [46–48]. Cycloalkenes and alkenes were also detected as reaction products, and their formation can be explained by the cyclization of chain fragments and cracking

reactions, respectively. Dehydrogenation of these cycloalkenes and alkenes leads to generate aromatic hydrocarbons [38,39], which could be the possible secondary reaction route promoted over Pd/NT-Ti. Additionally, these latter compounds could be formed from dealkylation reactions of p-cymene as was observed in DL-limonene pyrolysis with catalyst presence.

From styrene-butadiene rubber decomposition, secondary reactions as dehydrogenation, cyclization, and dealkylation could be responsible for the formation of BTX from 1,3-butadiene, cyclohexene, 4-ethenyl- and styrene. Similarly, from polybutadiene rubber is possible to obtain BTX by the same secondary reactions as those affecting alkenes and cycloalkenes generated from rubber depolymerized radicals [16,24]. Finally, it was demonstrated that Pd/NT-Ti favored the formation of BTX and p-cymene, owing to the conjugated presence of acid sites and highly dispersed Pd^0 nanoclusters. In fact, the catalyst was selective to monoaromatics while undesirable PAHs were not detected, which is significantly different from that previously used for the same reaction.

4. Conclusions

Catalytic pyrolysis of the waste tire using noble-metal-based catalysts on nanostructured support (titanates nanotubes) has been investigated here in relation to product distribution and yield of high-value hydrocarbons as BTX and p-cymene. The M/NT-Ti (M: Pd, Pt, or Au) catalysts exhibited low nanoparticle sizes ($1.8 < NPs < 2.2$ nm) and a homogeneous pore size distribution owing to the textural properties of the support. The catalyzed reaction strongly increased the formation of monoaromatic compounds in the following order Pd $>$ Pt $\approx$ Au $>$ support $>>$ non-catalyst. The Pd-catalyst demonstrated excellent activity for converting waste tire into monoaromatics-enriched oil by participating in the secondary reactions of dehydrogenation, cyclization, dealkylation, isomerization, and aromatization, and leading to a higher formation of BTX and p-cymene than the uncatalyzed reaction. Moreover, the bifunctional character of the catalyst may have a synergistic effect on the catalytic activity since the cyclization, isomerization, and aromatization reactions may be favored both over metallic and acid sites of the catalyst. Comprehensive reaction pathways describing the catalytic pyrolysis of the waste tire leading to the formation of these compounds over Pd/NT-Ti was proposed by studying the catalytic pyrolysis of individual polymers constituting the waste tires, and D,L-Limonene.

CRediT authorship contribution statement

Paula Osorio-Vargas: Conceptualization, Methodology, Investigation, Formal Analysis, Visualization, Project Administration, Funding Acquisition, Writing - original draft. **Cristian H. Campos:** Supervision, Conceptualization, Methodology, Writing - review & editing. **Cecilia C. Torres:** Methodology, Data curation, Resources. **Carla Herrera:** Data curation. **Krishnamoorthy Shanmugaraj:** Methodology, Data curation. **Tatiana M. Bustamante:** Data curation. **J.N. Diaz de Leon:** Data curation. **Francisco Medina:** Data curation. **Luis E. Arteaga-Pérez:** Conceptualization, Conceptualization, Supervision, Project Administration, Writing - review & editing, Funding Acquisition.

Declaration of Competing Interest

The authors declare that they have no known competing financial interests or personal relationships that could have appeared to influence the work reported in this paper.

Acknowledgements

The authors thank to Fondo Nacional de Desarrollo Científico y Tecnológico-FONDECYT (Chile) postdoctoral grant ID 3190610, postdoctoral grant ID 3210008, grant ID 1191465 and grant ID 1190063, and project Consejo Nacional de Ciencia y Tecnología-SENER-CONACyT (Mexico) grant ID 117373 for the financial support. C.C. Torres thanks to Comisión Nacional de Investigación Científica y Tecnológica-CONICYT (Chile), PAI/Concurso Nacional Inserción de Capital Humano Avanzado en la Academia Convocatoria año 2017 grant ID PAI 79170027.

Appendix A. Supporting information

Supplementary data associated with this article can be found in the online version at doi:10.1016/j.cattod.2021.06.029.

References

[1] WBCSD, Global ELT Management - A Global State of Knowledge on Collection Rates, Recovery Routes, and Management Methods, 2018.
[2] A. Mohajerani, L. Burnett, J.V. Smith, S. Markovski, G. Rodwell, M.T. Rahman, H. Kurmus, M. Mirzababaei, A. Arulrajah, S. Horpibulsuk, F. Maghool, Recycling waste rubber tyres in construction materials and associated environmental considerations: a review, Resour. Conserv. Recycl. 155 (2020), 104679, https://doi.org/10.1016/j.resconrec.2020.104679.
[3] G. Zhang, F. Chen, Y. Zhang, L. Zhao, J. Chen, L. Cao, J. Gao, Properties and utilization of waste tire pyrolysis oil: a mini review, Fuel Process. Technol. 211 (2021), 106582, https://doi.org/10.1016/j.fuproc.2020.106582.
[4] J. Xu, J. Yu, J. Xu, C. Sun, W. He, J. Huang, G. Li, High-value utilization of waste tires: a review with focus on modified carbon black from pyrolysis, Sci. Total Environ. 742 (2020), 140235, https://doi.org/10.1016/j.scitotenv.2020.140235.
[5] M. Arabiourrutia, G. Lopez, M. Artetxe, J. Alvarez, J. Bilbao, M. Olazar, Waste tyre valorization by catalytic pyrolysis – a review, Renew. Sustain. Energy Rev. 129 (2020), 109932, https://doi.org/10.1016/j.rser.2020.109932.
[6] D. Li, S. Lei, F. Lin, L. Zhong, W. Ma, G. Chen, Study of scrap tires pyrolysis – products distribution and mechanism, Energy 213 (2020), 119038, https://doi.org/10.1016/j.energy.2020.119038.
[7] P.T. Williams, A.J. Brindle, Catalytic pyrolysis of tyres: influence of catalyst temperature, Fuel 81 (2002) 2425–2434, https://doi.org/10.1016/S0016-2361(02)00196-5.
[8] P.T. Williams, A.J. Brindle, Fluidised bed pyrolysis and catalytic pyrolysis of scrap tyres, Environ. Technol. 24 (2003) 921–929, https://doi.org/10.1080/09593330309385629.
[9] P.T. Williams, A.J. Brindle, Aromatic chemicals from the catalytic pyrolysis of scrap tyres, J. Anal. Appl. Pyrolysis 67 (2003) 143–164, https://doi.org/10.1016/S0165-2370(02)00059-1.
[10] M. Arabiourrutia, M. Olazar, R. Aguado, G. López, A. Baron, J. Bilbao, HZSM-5 and HY zeolite catalyst performance in the pyrolysis of tires in a conical spouted bed reactor, Ind. Eng. Chem. Res. 47 (2008) 7600–7609, https://doi.org/10.1021/ie800376d.
[11] B. Shen, C. Wu, R. Wang, B. Guo, C. Liang, Pyrolysis of scrap tyres with zeolite USY, J. Hazard. Mater. 137 (2006) 1065–1073, https://doi.org/10.1016/j.jhazmat.2006.03.040.
[12] S. Boxiong, W. Chunfei, G. Binbin, W. Rui, Liangcai, Pyrolysis of waste tyres with zeolite USY and ZSM-5 catalysts, Appl. Catal. B Environ. 73 (2007) 150–157, https://doi.org/10.1016/j.apcatb.2006.07.006.
[13] M. Olazar, R. Aguado, M. Arabiourrutia, G. Lopez, A. Barona, J. Bilbao, Catalyst effect on the composition of tire pyrolysis products, Energy Fuels 22 (2008) 2909–2916, https://doi.org/10.1021/ef8002153.
[14] J. Wang, J. Jiang, X. Wang, P. Liu, J. Li, G. Liu, K. Wang, M. Li, Z. Zhong, J. Xu, A. J. Ragauskas, Catalytic conversion of rubber wastes to produce aromatic hydrocarbons over USY zeolites: effect of SiO_2/Al_2O_3 mole ratio, Energy Convers. Manag. 197 (2019), 111857, https://doi.org/10.1016/j.enconman.2019.111857.
[15] J. Yu, S. Liu, A. Cardoso, Y. Han, K. Bikane, L. Sun, Catalytic pyrolysis of rubbers and vulcanized rubbers using modified zeolites and mesoporous catalysts with Zn and Cu, Energy 188 (2019), 116117, https://doi.org/10.1016/j.energy.2019.116117.
[16] K. Ding, Z. Zhong, B. Zhang, J. Wang, A. Min, R. Ruan, Catalytic pyrolysis of waste tire to produce valuable aromatic hydrocarbons: an analytical Py-GC / MS study, J. Anal. Appl. Pyrolysis 122 (2016) 55–63, https://doi.org/10.1016/j.jaap.2016.10.023.
[17] S. Vichaphund, D. Aht-ong, V. Sricharoenchaikul, D. Atong, Effect of CV-ZSM-5, Ni-ZSM-5 and FA-ZSM-5 catalysts for selective aromatic formation from pyrolytic vapors of rubber wastes, J. Anal. Appl. Pyrolysis 124 (2017) 733–741, https://doi.org/10.1016/j.jaap.2016.11.011.
[18] N.A. Dũng, R. Klaewkla, S. Wongkasemjit, S. Jitkarnka, Light olefins and light oil production from catalytic pyrolysis of waste tire, J. Anal. Appl. Pyrolysis 86 (2009) 281–286, https://doi.org/10.1016/j.jaap.2009.07.006.
[19] N.A. Dũng, W. Tanglumlert, S. Wongkasemjit, S. Jitkarnka, Roles of ruthenium on catalytic pyrolysis of waste tire and the changes of its activity upon the rate of calcination, J. Anal. Appl. Pyrolysis 87 (2010) 256–262, https://doi.org/10.1016/j.jaap.2010.01.004.
[20] N.A. Dũng, S. Wongkasemjit, S. Jitkarnka, Effects of pyrolysis temperature and Pt-loaded catalysts on polar-aromatic content in tire-derived oil, Appl. Catal. B Environ. 91 (2009) 300–307, https://doi.org/10.1016/j.apcatb.2009.05.038.

[21] W. Namchot, S. Jitkarnka, Impacts of nickel supported on different zeolites on waste tire-derived oil and formation of some petrochemicals, J. Anal. Appl. Pyrolysis 118 (2016) 86–97, https://doi.org/10.1016/j.jaap.2016.01.001.
[22] P. Osorio-Vargas, T. Menares, D. Lick, M.L. Casella, R. Romero, R. Jiménez, L. E. Arteaga-Pérez, Tuning the product distribution during the catalytic pyrolysis of waste tires: the effect of the nature of metals and the reaction temperature, Catal. Today (2020), https://doi.org/10.1016/j.cattod.2020.10.035.
[23] K. Ding, Z. Zhong, B. Zhang, Z. Song, X. Qian, Pyrolysis characteristics of waste tire in an analytical pyrolyzer coupled with gas chromatography/mass spectrometry, Energy Fuels 29 (2015) 3181–3187, https://doi.org/10.1021/acs.energyfuels.5b00247.
[24] F. Xu, B. Wang, D. Yang, X. Ming, Y. Jiang, J. Hao, Y. Qiao, Y. Tian, TG-FTIR and Py-GC/MS study on pyrolysis mechanism and products distribution of waste bicycle tire, Energy Convers. Manag. 175 (2018) 288–297, https://doi.org/10.1016/j.enconman.2018.09.013.
[25] R.B. Dinamarca, R. Espinoza-González, C.H. Campos, G. Pecchi, Magnetic Pt single and double core-shell structures for the catalytic selective hydrogenation of cinnmaladehyde, Pure Appl. Chem. 92 (2020) 413–427, https://doi.org/10.1515/pac-2018-1227.
[26] K. Shanmugaraj, T.M. Bustamante, C.C. Torres, C.H. Campos, Gold nanoparticles supported on mesostructured oxides for the enhanced catalytic reduction of 4-nitrophenol in water, Catal. Today (2020), https://doi.org/10.1016/j.cattod.2020.05.051.
[27] R. Cid, G. Pecchi, Potentiometric method for determining the number and relative strength of acid sites in colored catalysts, Appl. Catal. 14 (1985) 15–21.
[28] T.M. Bustamante, C.H. Campos, M.A. Fraga, J.L.G. Fierro, G. Pecchi, Promotional effect of palladium in Co-SiO_2 core@shell nanocatalysts for selective liquid phase hydrogenation of chloronitroarenes, J. Catal. 385 (2020) 224–237, https://doi.org/10.1016/j.jcat.2020.03.006.
[29] T. Menares, J. Herrera, R. Romero, P. Osorio, L.E. Arteaga-Pérez, Waste tires pyrolysis kinetics and reaction mechanisms explained by TGA and Py-GC/MS under kinetically-controlled regime, Waste Manag. 102 (2020) 21–29, https://doi.org/10.1016/j.wasman.2019.10.027.
[30] B. Klemetsrud, J. Klinger, E. Bar Ziv, D. Shonnard, A kinetic study of the fast micro-pyrolysis of hybrid poplar, J. Anal. Appl. Pyrolysis 128 (2017) 353–362, https://doi.org/10.1016/j.jaap.2017.09.014.
[31] P.T. Williams, S. Besler, Pyrolysis-thermogravimetric analysis of tyres and tyre components, Fuel 74 (1995) 1277–1283.
[32] G.S. Miguel, J. Aguado, D.P. Serrano, J.M. Escola, Thermal and catalytic conversion of used tyre rubber and its polymeric constituents using Py-GC/MS, Appl. Catal. B Environ. 64 (2006) 209–219, https://doi.org/10.1016/j.apcatb.2005.12.004.
[33] M. Kitano, E. Wada, K. Nakajima, S. Hayashi, S. Miyazaki, H. Kobayashi, M. Hara, Protonated titanate nanotubes with Lewis and Brønsted acidity: relationship between nanotube structure and catalytic activity, Chem. Mater. 25 (2013) 385–393, https://doi.org/10.1021/cm303324b.
[34] R. Camposeco, S. Castillo, I. Mejía-Centeno, J. Navarrete, J. Marín, Characterization of physicochemical properties of Pd/TiO_2 nanostructured catalysts prepared by the photodeposition method, Mater. Charact. 95 (2014) 201–210, https://doi.org/10.1016/j.matchar.2014.06.017.
[35] G.J. Kim, D.W. Kwon, S.C. Hong, The effect of Pt particle size and valence state on the performance of Pt/TiO_2 catalysts for CO oxidation at room temperature, J. Phys. Chem. C 120 (2016) 17996–18004, https://doi.org/10.1021/acs.jpcc.6b02945.
[36] N. Lakshmanareddy, V. Navakoteswara Rao, K.K. Cheralathan, E.P. Subramaniam, M.V. Shankar, Pt/TiO_2 nanotube photocatalyst – effect of synthesis methods on valance state of Pt and its influence on hydrogen production and dye degradation, J. Colloid Interface Sci. 538 (2019) 83–98, https://doi.org/10.1016/j.jcis.2018.11.077.
[37] R. Camposeco, S. Castillo, M. Hinojosa-Reyes, I. Mejía-Centeno, R. Zanella, Surface acidity, adsorption capacity, and photocatalytic activity of SiO_2 supported on TiO_2 nanotubes for Rhodamine B degradation, Top. Catal. 64 (2021) 84–96, https://doi.org/10.1007/s11244-020-01339-3.
[38] H. Pines, The Chemistry of Catalytic Hydrocarbon Conversions, 1982. https://doi.org/10.1016/0166–9834(82)80102–4.
[39] G. Busca, Metal catalysts for hydrogenations and dehydrogenations, Heterog. Catal. Mater. (2014) 297–343, https://doi.org/10.1016/b978-0-444-59524-9.00009-2.
[40] A. Corma Canos, S. Iborra, A. Velty, Chemical routes for the transformation of biomass into chemicals, Chem. Rev. 107 (2007) 2411–2502, https://doi.org/10.1021/cr050989d.
[41] J. Wang, J. Jiang, X. Wang, S. Pang, Y. Sun, X. Meng, M. Li, R. Ruan, A. J. Ragauskas, Enhanced BTEX formation via catalytic fast pyrolysis of styrene-butadiene rubber: comparison of different catalysts, Fuel 278 (2020), 118322, https://doi.org/10.1016/j.fuel.2020.118322.
[42] C. Tavera-Ruiz, P. Gauthier-Maradei, M. Capron, D. Ferreira-Beltran, C. Palencia-Blanco, J.C. Morin, F. Dumeignil, An alternative to the cymenes production from scrap tire rubber using heteropolyacid catalysts, Waste Biomass Valorization 10 (2019) 3057–3069, https://doi.org/10.1007/s12649-018-0310-1.
[43] S.S. Choi, D.H. Han, Pyrolysis paths of polybutadiene depending on pyrolysis temperature, Macromol. Res. 14 (2006) 354–358, https://doi.org/10.1007/BF03219094.
[44] J. Ackermann, E. Klemm, G. Emig, Synthesis of ethylbenzene from 1,3-butadiene using basic zeolite catalysts, Stud. Surf. Sci. Catal. 130 A (2000) 863–868, https://doi.org/10.1016/s0167-2991(00)81067-8.
[45] J.S. Chang, S.E. Park, Q. Gao, G. Férey, A.K. Cheetham, Catalytic conversion of butadiene to ethylbenzene over the nanoporous nickel(II) phosphate, VSB-1, Chem. Commun. (2001) 859–860, https://doi.org/10.1039/b009160j.
[46] D. Buhl, D. Roberge, W. Holderich, Production of p-cymene from α-limonene over silica supported Pd catalysts, Appl. Catal. A Gen. 188 (1999) 287–299.
[47] C. Zhao, W. Gan, X. Fan, Z. Cai, P.J. Dyson, Y. Kou, Aqueous-phase biphasic dehydroaromatization of bio-derived limonene into p -cymene by soluble Pd nanocluster catalysts, J. Catal. 254 (2008) 244–250, https://doi.org/10.1016/j.jcat.2008.01.003.
[48] R.J. Grau, P.D. Zgolicz, C. Gutierrez, H.A. Taher, Liquid phase hydrogenation, isomerization and dehydrogenation of limonene and derivatives with supported palladium catalysts, J. Mol. Catal. A Chem. 148 (1999) 203–214, https://doi.org/10.1016/S1381-1169(99)00108-9.